ARTICLE

Wireless Self-Powered High-Performance Integrated Nanostructured-Gas-Sensor Network for Future Smart Homes

Zhilong Song,[‡] Wenhao Ye,[‡] Zhuo Chen, Zhesi Chen, Mutian Li, Wenying Tang, Chen Wang, Zhu'an Wan, Swapnadeep Poddar, Xiaolin Wen, Xiaofang Pan, Yuanjing Lin, Qingfeng Zhou, and Zhiyong Fan*

Cite This: *ACS Nano* 2021, 15, 7659−7667

Read Online

ACCESS | Metrics & More | Article Recommendations | Supporting Information

ABSTRACT: The accelerated evolution of communication platforms including Internet of Things (IoT) and the fifth generation (5G) wireless communication network makes it possible to build intelligent gas sensor networks for real-time monitoring chemical safety and personal health. However, this application scenario requires a challenging combination of characteristics of gas sensors including small formfactor, low cost, ultralow power consumption, superior sensitivity, and high intelligence. Herein, self-powered integrated nanostructured-gas-sensor (SINGOR) systems and a wirelessly connected SINGOR network are demonstrated here. The room-temperature operated SINGOR system can be self-driven by indoor light with a Si solar cell, and it features ultrahigh sensitivity to

H_2, formaldehyde, toluene, and acetone with the record low limits of detection (LOD) of 10, 2, 1, and 1 ppb, respectively. Each SINGOR consisting of an array of nanostructured sensors has the capability of gas pattern recognition and classification. Furthermore, multiple SINGOR systems are wirelessly connected as a sensor network, which has successfully demonstrated flammable gas leakage detection and alarm function. They can also achieve gas leakage localization with satisfactory precision when deployed in one single room. These successes promote the development of using nanostructured-gas-sensor network for wide range applications including smart home/building and future smart city.

KEYWORDS: *3D nanostructured tin oxide, gas sensor network, self-powered device, machine learning algorithm, smart home*
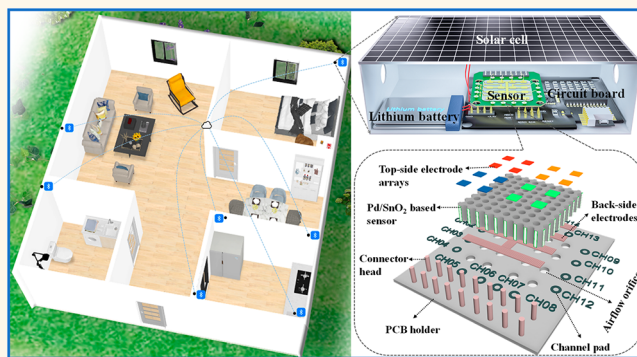
INTRODUCTION

Chemical sensors play critical roles in a smart and sustainable city where a safe and healthy environment is the foundation.[1−3] The rapid advancement of IoT technology and 5G communication in a smart city and smart home/building promotes the development of high-performance sensors and intelligent sensor networks to monitor flammable and toxic gases, *e.g.*, H_2, CO, NO_2, formaldehyde, toluene, *etc.*, in our environment with high accuracy and spatial resolution in order to trigger subsequent air purification.[4−7] In fact, to construct an intelligent sensor network with a large number of sensor nodes, an ensemble of compulsory characteristics of gas sensors including small formfactor, low cost, ultralow power consumption, high sensitivity, and high intelligence is required. In principle, solid-state gas sensors, especially metal oxide (MOX)-based gas sensors, are good candidates for this application. However, their wide adoption in the aforemen-

tioned sensor network is largely limited by the sensor selectivity and high-power consumption ($10^1−10^3$ mW) from the mandatory heaters integrated with the sensors.[1,8] Therefore, the development of ultralow-power consumption gas sensors is of paramount importance for future smart applications.

Gas sensors based on three-dimensional (3D) nanostructured materials have been reported and demonstrated to achieve room-temperature gas-sensing performance with low power consumption, but with modest detection limits.[9−11]
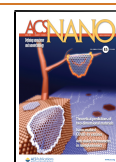
Apart from research efforts in material and device engineering, pattern recognition algorithms that aim to classify the input values based on the "training process" with data regularities have demonstrated themselves as the effective strategies for complicated gas sensing signal decoding.[12,13] To realize sufficient data input and enhance the decoding accuracy, sensor arrays and data communication are required.[14−17] In this regard, power regulation and energy savings are essential to achieve a smart sensor network with long operational durability. Self-powered systems that employ power sources of solar energy, mechanical vibration, bioenergy, wind flow and thermal energy, *etc.* have been widely demonstrated as efficient approaches to realize sustainable gas sensor nodes.[18−22] However, indoor-light-driven self-powered gas sensor array systems for smart home/building applications have not been previously reported,[23,24] mainly due to the challenges on system integration of different functional modules and the stringent requirement on power consumption of gas sensors, which is beyond the capability of indoor light sources (power density <1000 μW cm^{-2}).[20]

Herein, we developed an indoor-light-driven self-powered integrated nanostructured-gas-sensor (SINGOR) system with high-performance 3D nanostructured palladium (Pd) decorated SnO$_2$ sensor arrays, and it was employed to construct a wireless smart gas sensing network with ultralow power consumption for smart home applications (Figure 1a−c). In general, the SINGOR system consists of a power supply module, gas-sensing module, microcontroller-analog readout circuit, and wireless data transmission module. The sensors

were constructed on 3D nanoporous anodic aluminum oxide (AAO) templates coated with an ultrathin and conformal layer of SnO$_2$ thin film with atomic layer deposition (ALD) followed by deposition of a conformal Pd layer also with ALD. Various metals were used as electrodes to achieve a sensor array (Figure 1c). The as-fabricated sensors achieved ultrahigh sensitivity toward H$_2$, formaldehyde, toluene, and acetone in ultralow concentrations at room temperature, which was ascribed to the high surface area and additional catalytic effects from the decorated Pd nanoparticles. Thus, the average power consumption of each sensor module was dramatically reduced to 4.3 μW, which is 3 orders of magnitude lower than that of commercial SnO$_2$-based sensors at the milliwatt level. Owing to the ultralow power consumption of sensor devices, a solar cell was used in the system enabling indoor-light energy to electricity conversion for sustaining the system operation. The generated electricity could also be simultaneously stored in the integrated lithium-ion battery to serve as the backup power supply under dark conditions. Meanwhile, multiple SINGOR systems can be spatially deployed in a smart home as a sensor network (Figure 1a) and connected with a smartphone through Bluetooth, which can achieve continuous and sustainable remote monitoring of the complex gaseous environments with visualization on the mobile app (Figure 1b). Moreover, the assembled sensor arrays could realize gas recognition and gas leakage source tracing based on a machine learning algorithm. Rational power management strategies such a self-powered energy module ensure a sustainable and stable power supply for full system functions without external power sources and eliminate environmental interferences. The as-developed SINGOR system is highly attractive for real-time and continuous monitoring of targeted gas to ensure indoor environment safety in future smart home and building applications.

RESULTS AND DISCUSSION

Sensor Fabrication and SINGOR System Design. The sensor array devices based on 3D nanoporous AAO templates (Figure S1b,c) were primarily fabricated by ALD method. The freestanding nanoporous AAO templates provide a large surface-to-volume ratio with 50 μm thickness, 500 nm pitch, and 400 nm average pore size. The low-temperature operated ALD could achieve uniform and conformal thin film deposition with a precise thickness control on 3D surfaces, which is crucial for achieving high device yield and desirable repeatability on the AAO substrate.[25−27] In the ALD process for SnO$_2$ deposition (Figure S1), alternative pulses of two precursors vapor tetrakis(dimethylamino)tin (TDMAS) and H$_2$O and purge N$_2$ gas were introduced into the reactor. The self-saturating reactions then led to the self-limited growth of amorphous SnO$_2$ thin film on the 3D AAO substrate. After this, an annealing treatment (450 °C, 3 h in air) of the SnO$_2$ thin film was conducted, and the intrinsic SnO$_2$ was formed whose compactness could be clearly observed on the side wall inside AAO channels with a thickness of ∼12 nm (Figures S1d,e and S2a). Here, 3D SnO$_2$ architecture substantially increases the device surface area, thus leading to more effective interaction with the gas molecules in the environment. To further improve device sensing performance, a ∼3 nm layer of Pd nanoparticle decoration (Figure S2b) was deposited by the ALD process (Methods) to incorporate metal catalytic effect and promote surface reaction with the target gas species. Figure S2c shows that the Pd (111) peak appeared in the XRD
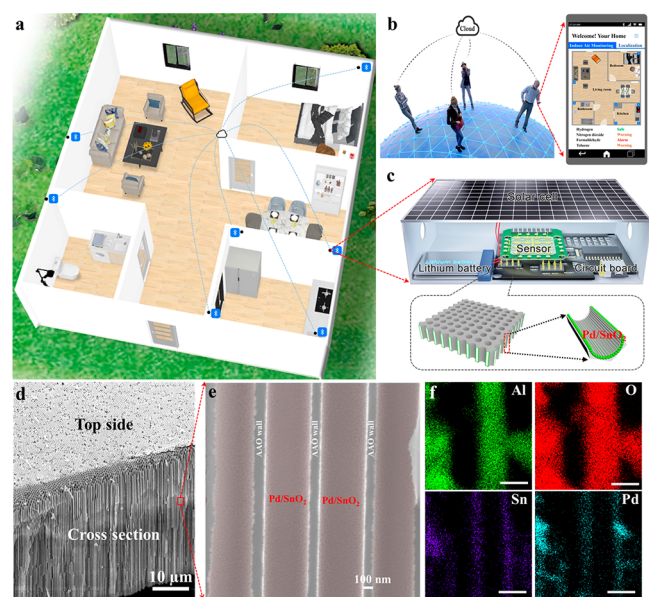
Figure 1. Schematic of SINGOR network in the smart home application. (a) Layout of the gas sensor array network in a smart home. (b) Remote monitoring in different locations using a smart mobile phone. (c) SINGOR system components consisting of a power supply module (solar cell and the lithium-ion battery), gas-sensing module (magnified view of the 3D nanostructured Pd/SnO$_2$ thin films on AAO substrate is also shown with dotted arrow markers), microcontroller-analog readout circuit and wireless data transmission module on a PCB board. (d, e) SEM images of the cross sections of Pd/SnO$_2$ thin films. (f) Element mapping of the Al, O, Sn, Pd dispersion from the cross sections of the Pd/SnO$_2$ thin films (scale bar: 100 nm).
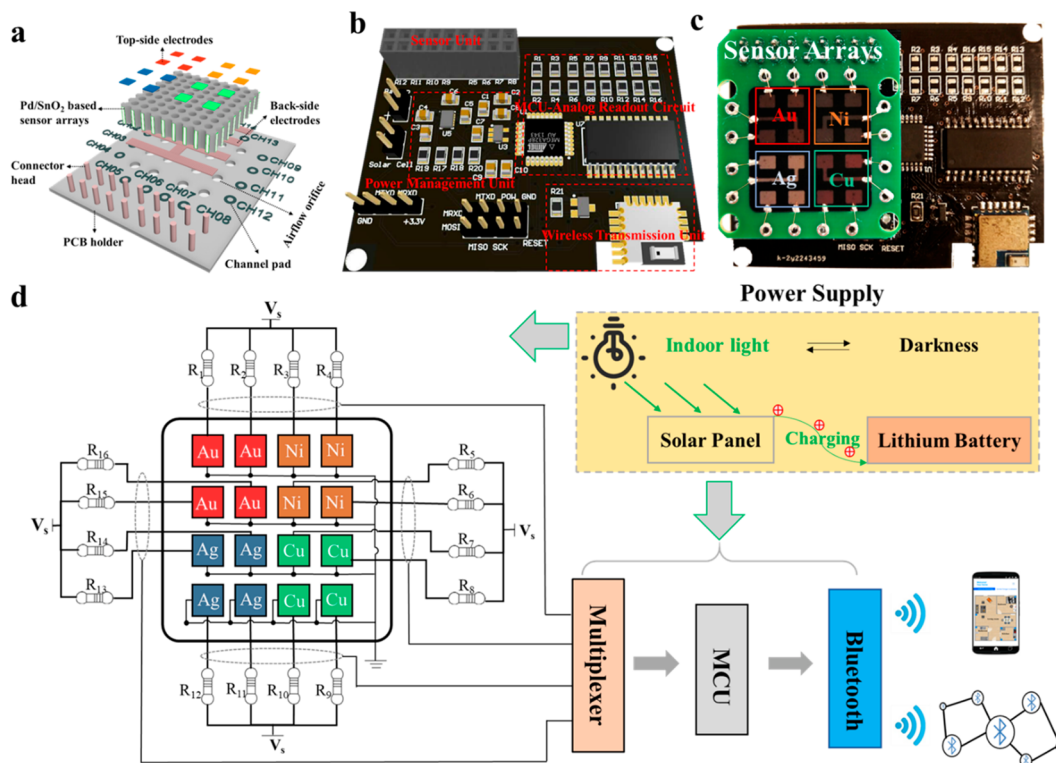
Figure 2. Illustration of SINGOR system: (a) gas sensor array packaging structure; (b) readout circuitry; (c) integrated sensor arrays on the circuit board; (d) schematic of the whole wireless indoor-light-driven SINGOR system.

spectra (red curve in Figure S2) after Pd ALD on SnO_2/AAO, confirming the successful Pd nanoparticle decoration. SEM images (Figure 1d) showed the cross-section of the AAO substrate with Pd-decorated intrinsic SnO_2 thin film (Pd/SnO_2). We can observe a uniform Pd/SnO_2 thin film in all of the channels (Figure 1e) with an average thickness of 15 nm. The uniformity of the Pd/SnO_2 thin film was also confirmed in the element mapping images of the Al, O, Sn, and Pd dispersion (Figure 1f).

In order to improve the capability of gas recognition and classification, a 4 × 4 sensor array (Figure 2a) was fabricated in which each-type sensor module showed specific sensing behavior toward the target gas. Specifically, four kinds of metals, namely gold (Au), copper (Cu), nickel (Ni), and silver (Ag), were patterned as 16 top electrodes on the as-fabricated 3D Pd/SnO_2/AAO substrate. A vertical array device structure was completed together with the common ground Au bottom electrode as shown in Figure 2a. A readout printed circuit board (PCB) was designed and fabricated (Figure 2b) to integrate the sensor module, single processing module, signal transmission module, and power supply module. The PCB has a microcontroller (MCU, ATMega328P) for data acquisition and analog−digital conversion and a bluetooth low energy (BLE) unit (WH BLE-103) for wireless transmission. Specifically, the MCU acquires the voltage signals of each sensor (from channel 0 to 15) through a multiplexer (CD-HC4067), and the signals are then converted into corresponding digital values for data transmission. The BLE unit enables the wireless connection between the sensor module and the terminal devices, such as mobile phones, computers, and cloud servers. The sensing signals are then analyzed with principal component analysis (PCA) and support vector machine (SVM) algorithms and visualized on the mobile app, displaying

the gas species and concentration levels at different locations. Figure 2c shows a photo of a real device with PCB circuit board. A commercial monocrystalline solar cell panel (4 cm × 11 cm) and a rechargeable lithium-ion battery (800 mA·h) were further assembled to provide sustainable power supply. The block diagram and photos of a fully integrated SINGOR system are exhibited in Figure S4. The working mechanism of the SINGOR system is illustrated in Figure 2d, and the detailed circuit designs are provided in the Supporting Information (Figure S5a).

One bottleneck challenge for indoor self-powered devices driven by solar cells is that the indoor light intensity under normal illuminance is typically less than 1 mW/cm^2 (Table S1), and thus, the on-board solar cell cannot provide high power and a low power device design is critically important. Here, our SINGOR system features ultralow power consumption, and it can operate in a self-powered fashion with rational power management. Specifically, when the indoor light is on, the system is operated in an intermittent mode which draws power from both solar cell panel and lithium-ion battery in working cycles, and it allows recharging of the lithium-ion battery in the power down cycles with the solar cell, as illustrated in Figure S5b. On the other hand, the power management module of the sensor system will disable the charging function automatically without sufficient indoor light illumination, and the lithium-ion battery will serve as a backup electrochemical energy source to support the normal operation of the SINGOR system in a continuous sensing mode. In reality, the solar cell has a conversion efficiency of 12% under 1000 μW cm^{-2} input power density with the distance of 10 cm to the indoor light source (Figure S5c1). The lithium-ion battery discharging and charging behavior with light irradiation off and on were characterized, demonstrating that the solar cell

could harvest enough power for charging the lithium-ion battery and operating the sensor system sustainably (Figure S5c2). To overcome the output power fluctuation of solar cells due to the indoor-light intensity variation and ambient temperature, a low drop-out linear voltage regulator (TPS7A05) and a solar-cell-lithium-ion-battery charging integrated circuit (BQ24210) were utilized to ensure a constant voltage output of 3.3 V for the system operation (Figure S5b). The total power consumption of the system with all the 16 sensors in operation is about 26 mW for continuous sensing mode. The power output of the solar cell is typically around 5.3 mW. The average power consumption of our sensor system can be further lowered down by setting different duty cycles of the intermittent mode (Table S2). Specifically, during on cycles, the power consumption of the system remains at 12.87 mW (3.9 mA*3.3 V) with the bluetooth turned on and executing wireless communication function. During off cycles, the MCU enters sleep mode and consumes an average power of 313.5 μW (95 μA, 3.3 V), while the bluetooth unit is shut down automatically by the MCU and consumes almost no power. Hence, as the duty cycle continues to decrease, the power consumption of the system is mainly from the MCU and the sensor unit, and the minimal power consumption of the system can be as low as around 382.1 μW. Notably, our sensor array (16 sensors) can operate at room temperature with an ultralow-power consumption of 68.6 μW, which is much lower than those of the traditional commercial gas sensors at mW level and the state-of-art commercial low-power MEMS gas sensors (Table S3).

Room-Temperature Gas-Sensing Performance Based on the SINGOR System. Sensing performance of the as-fabricated Pd/SnO$_2$ based gas sensors was characterized at room temperature. The study of the impact of AAO pore size and thickness on the gas-sensing performance was carried out, and the best gas-sensing performance has been achieved by employing the AAO template with 50 μm thickness and 400 nm average pore size (Figure S6). Overall, more internal surface area enhances device response. An optimized geometry (pore size and thickness) could be obtained when taking the molecular mean free-path and gas diffusion model into consideration, which needs further investigation. The thickness of deposited SnO$_2$ thin film and catalytic effect with Pd nanoparticle decoration were studied and optimized for detection of H$_2$, which is highly flammable and explosive with the concentration exceeding 40000 ppm in air and thus requires highly sensitive leakage detection.[28,29] Monitoring H$_2$ leakage in a smart home in Hong Kong is also of practical importance as 40% of the town gas is H$_2$. The thickness of SnO$_2$ thin films can be precisely controlled by the number of ALD cycles, and it was discovered that the SnO$_2$ thin film-based gas sensor with 45 cycles deposition (~12 nm, Figure S2) features the optimal response toward H$_2$ from 20 to 1000 ppm (Figure S7). Therefore, 3 nm thick Pd decoration was deposited on this kind of SnO$_2$/AAO device with ALD as well. As demonstrated in Figure S7, the Pd/SnO$_2$/AAO based gas sensor shows dramatic enhancement (~62.7 times) of response (144.2@1000 ppm) compared with that of the pristine SnO$_2$ ones (2.3@1000 ppm). Such a substantial sensing response enhancement can be ascribed to the catalytic effect at the Pd−SnO$_2$ interface which can be explained by the chemical and electronic sensitization promoted by the Pd nanoparticles decoration.[30,31] In this chemical sensitization process, oxygen molecules can easily adsorb on the Pd/SnO$_2$

surface, and then they are converted to active ionic species (O$_2^-$, O$^-$, and O^{2-}) by capturing electrons from the SnO$_2$ surface, producing the surface electron depletion region, and resulting in the high resistance baseline in air.[32] When exposed to the H$_2$ atmosphere, the H$_2$ dissociation (H$_2 \rightarrow$ 2H) will be catalyzed on the Pd nanoparticle surface and the dissociated H atoms migrate to the Pd−SnO$_2$ interface *via* a spillover effect,[33,34] reducing the preadsorbed oxygen ions. Then the released electrons from the oxygen ions transfer back to the conduction band of SnO$_2$, contributing to the decrease of the sensor's resistance and ultimately enhancing the sensitivity. In addition to this oxygen ion reduction mechanism, Pd work function reduction can also contribute to sensitivity enhancement. As shown in Figure S8, Pd-decorated SnO$_2$ is known to have a Schottky junction at the interface because of the work function difference. It leads to an electron depletion region at the Pd−SnO$_2$ interface. Intriguingly, Pd nanoparticles can easily transform into hydride form reversibly, *i.e.*, PdH$_x$ in H$_2$ atmosphere[35] with a lower work function. As PdH$_x$ has lower work function than Pd, it facilitates electron transfer back to SnO$_2$, thus decreasing the width of the electron depletion region, which essentially results in the gas-sensing performance improvement.[36]

The catalytic effect at the Pd−SnO$_2$ interface for gas sensing has been further studied in this work. Figures 3a and S9a show the typical real-time H$_2$ sensing curves of the four Pd/SnO$_2$-based gas sensors employing four kinds of metal (Au, Cu, Ni, Ag) electrodes.[37] The corresponding responses were extracted from the sensing curves and plotted in Figure 3b. These results demonstrate that the 3D Pd/SnO$_2$/AAO sensors have a very wide sensing response range for H$_2$ detection from 10 to 40000 ppm with largely enhanced response at room temperature, achieving the record low limit of detection (LOD) (Table S4), which enables an early state gas detection at the beginning of leakage event. Our sensors also show relatively good long-term stability for H$_2$ sensing in a month without obvious deterioration (Figure S10); however, more efforts should be further made to perform much prolonged stability study (response deterioration, baseline drift, *etc.*) for practical applications in the future. Apart from H$_2$ detection, the as-fabricated sensors were also tested for formaldehyde, toluene, and acetone sensing. These volatile organic compounds (VOCs) are the primary pollution gases that affect indoor air quality. The dynamic response and recovery curves were recorded (Figure 3c,e,g and Figure S9b−d), and the corresponding responses are displayed in Figure 3d,f,h. The Pd/SnO$_2$-based sensors have also achieved the record sensing performance toward formaldehyde, toluene, and acetone, with the LODs down to 2, 1, and 1 ppb, respectively, at room temperature. We also attribute the enhanced gas-sensing performance toward these VOCs to the spillover effect as mentioned above.[33,34] Here, Pd decoration promotes the adsorption and activation of the analyte gas, followed by the transfer of the activated species to the SnO$_2$ surface and reaction of the analyte gas with active oxygen from the SnO$_2$ surface, thus returning the captured electrons back to the SnO$_2$ surface. The LODs of the as-fabricated Pd/SnO$_2$-based sensors are benchmarked against previously reported room-temperature sensors (Tables S5−7), demonstrating their promising applications for real-time gas monitoring at room temperature with low power consumption. It is known that humidity effect has a significant influence on the sensor baseline signal and gas-sensing properties especially for those gas sensors
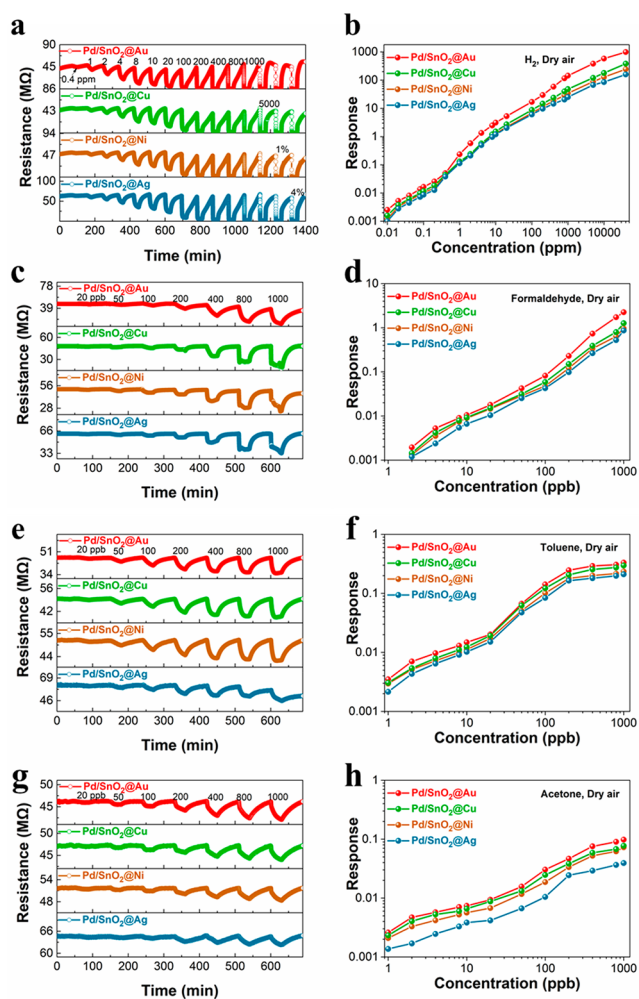
Figure 3. Room-temperature gas sensing properties (dry air) based on the 3D nanostructure gas sensor arrays. Sensing curves and response toward (a, b) H_2 from 10 ppb to 4%; (c, d) formaldehyde from 2 to 1000 ppb; (e, f) toluene from 1 to 1000 ppb; and (g, h) acetone from 1 to 1000 ppb.

operating at room temperature.[38,39] Therefore, the studies of humidity effects of our sensors toward H_2, formaldehyde, toluene, and acetone at 30%, 60%, and 85% relative humidity (RH) have also been carried out, respectively (Figure S11–13). These data demonstrate that the sensors could operate normally at different RH yet with a minor deterioration of the LOD at high RH. For these sensors, Pd catalytic effect dominates the sensing performance in the whole gas-sensing concentration ranges because of their appropriate activation capacity, so that the amount of H_2O molecules adsorbed on the Pd nanoparticle surface will only occupy part of the active sites and result in a reduced response.[40,41]

SINGOR System for Gas Discrimination and Classification. The sensor arrays with different metal electrodes were further utilized as a practical "smart electronic nose" system for multigases discrimination. Principal component analysis (PCA) and support vector machine (SVM) algorithms were employed by extracting the characteristic sensing signals from the sensor arrays for further data processing.[42,43] First, the responses of the four targeted gases in the concentration gradient were recorded and processed to build the database. The recorded four-dimensional data (corresponding to four kinds of gas sensors) was reduced to two-dimensional data by

PCA, which was used to visualize the response's Euclidean distance and relatedness intuitively among gas species as presented by the points located in Figure 4. It shows that each
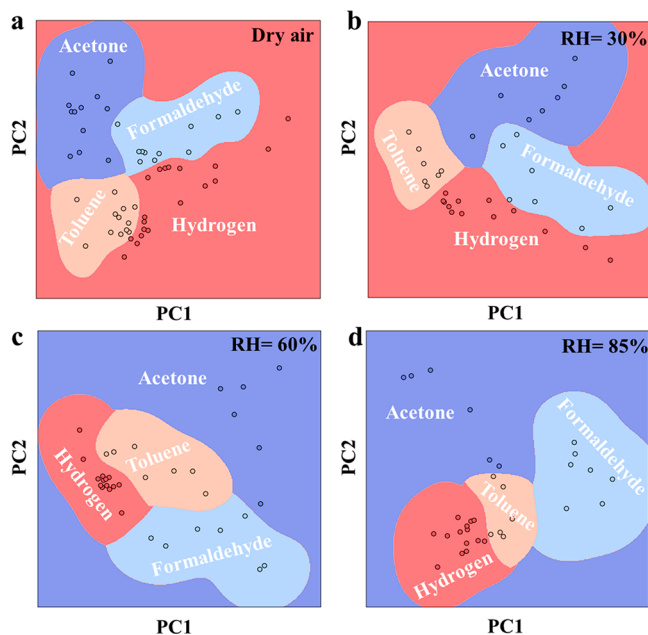
Figure 4. Gas classification of H_2, formaldehyde, toluene, and acetone in different relative humidities: (a) dry air, (b) RH = 30%, (c) RH = 60%, (d) RH = 85%, employing support vector machine (SVM) algorithms.

distinct gas can be deciphered from their respective circled clusters. Next, the SVM algorithm was further employed for gas discrimination, which can give a decision space for automatic unknown gas classification. The decision space for each gas is represented by one color. In reality, when an unknown gas interacts with the sensor array, the similarity of the sensing signal compared with the gases in the database is calculated following the kernel function below

$$K(x, x') = \exp[-\gamma(x - x')^2] \quad (1)$$

where x is the label of the unknown gas, x' is the label of one of the tested gases in the database, and γ is a constant which defines how far the influence of a single sample reaches.

If the unknown gas has high similarity to any specific gas in the database, the result of kernel function $K(x,x')$ tends to approach 1; otherwise, it is close to 0. In this fashion, each sensing signal can be processed and classified into specific gas species by comparison with the entire database following the decision function

$$\sum_{i=1}^{n} (\alpha_i - \alpha_i')K(x, \alpha_i') + \rho \quad (2)$$

where α is the dual coefficient (α determines the direction of the measured gases cluster) and ρ is the intercept (ρ determines the position of measured gases cluster); both are determined by the database. Finally, the unknown gas detected by the sensor array will be classified into the specific gas species with the highest score in the decision function. Moreover, PCA and SVM algorithms have also been successfully employed for multigases discrimination in different relative humidity. The target gases in different RH (dry air,

30%, 60%, and 85%) could be treated as one kind of distinct gas with its own cluster as shown in Figure 4a−d. Furthermore, the gases' concentrations and their corresponding responses follow the power-law function as shown in Figure S14, and the concentration of the target gases can be calculated by the fitting power-law function. Finally, both the concentration and types of unknown gases as well as RH can be determined by our sensor arrays with little or even no prior knowledge of gases, which can help to address the challenging issues of humidity effect and realize accurate gas detection in a complicated environment.

SINGOR Network for Future Smart Home. In a smart home/building, air quality real time monitoring with sufficient spatial resolution is in imminent need. Our high performance SINGOR system provides a potential solution for that particular application. In this work, a smart sensing network for real-time and continuous indoor gas environmental monitoring has been constructed with multiple SINGORs. The SINGORs were deployed in the living room, kitchen, bedroom, and bathroom, respectively, as shown in Figure 5a.

Figure 5. Smart home demonstration. (a) SINGOR systems deployed in the living room, kitchen, bedroom, and bathroom, respectively. (b) Cross-room real-time gas monitoring with the mobile app. (c) Four SINGOR systems deployed at the corners of the kitchen (bottom view). (d) Gas leakage source localization with red circle flashing shown in the mobile app.

The sensing signals were recorded and transmitted to a smartphone in real time *via* a wireless bluetooth protocol. Simultaneously, the MCU computed the responses of each sensor toward the exposed gases based on sensor resistance variation. Following the signal processing with PCA and SVM algorithms, the gas types and concentration levels were also determined by comparison with the database and visualized by the mobile app. Figure 5b shows that our SINGOR system

possesses the respectable fast response and recovery speed for real-time H_2 leakage detection, which can be clearly observed from Videos 1 and 2.

Moreover, we have found that the location coordinates of the gas leakage source can also be determined with the smart sensor network. Specifically, four SINGOR nodes were deployed at the corners of the kitchen (1.2 m × 2.3 m × 2.5 m) and kept at the same height (Figure 5c). By employing the gas diffusion model and gas leakage source localization algorithm (Figure S15), the gas leakage source location can be computed according to the sensing response changing rate at a certain gas concentration (α_c) and coordinates of each SINGOR node, which is described in detail in Figure S16. Note that here 100 ppm of H_2 is set to be the alarm threshold for indoor H_2 source leakage detection in our work. For simplicity, the distance indicator (α_c) of each sensor node is computed around 100 ppm of H_2 by selecting the nearest monitored concentration below and above 100 ppm and the corresponding sampling time interval Δt (time difference between two selected monitored concentration, here equals to 1s), and the relationship between α_c and r (the distance between SINGOR node and the leakage source) was obtained (Figure S17). Hence, the distance r between each sensor node inside the network can be computed by utilizing the relationship between α_c and r, together with the coordinates of each sensor node. Then the gas leakage source position can be determined with high accuracy and exhibited as a red circle flashing in the mobile app (Figure 5d and Video 3). Note that gas leakage localization can be difficult in a real situation when there is air turbulence in the room. Although it is beyond the scope of this work, the results here suggest the potential benefits of employing sensor network for gas leakage source localization.

CONCLUSIONS

In summary, we have successfully developed an indoor-light-driven SINGOR system by integrating a high-performance gas sensing module, power supply module with self-powered capability, MCU for data processing, and bluetooth unit for wireless data transmission. By integrating with a solar cell and a lithium-ion battery, the system achieved self-power capability in relatively low light intensity indoor ambience, making it practical for indoor environmental monitoring. Notably, the nanostructured $Pd/SnO_2/AAO$ sensors feature a high surface-area-to-volume ratio for effective surface interaction with gas molecules further enhanced by surface catalytic activity. This contributed to high sensing performance at room temperature. In particular, the as-fabricated sensors have achieved record low limits of detection toward H_2 (10 ppb), formaldehyde (2 ppb), toluene (1 ppb), and acetone (1 ppb) with low power consumption. The sensor array strategy has been harnessed to achieve gas classification with the aid of machine learning algorithms. Eventually, a smart gas sensing network was constructed and smart home applications on gas leakage alarming and localization have been successfully demonstrated. Overall, such a self-powered and wireless smart sensor network can play a vital role in future smart and healthy living.

METHODS

3D Pd/SnO$_2$ ALD. The SnO_2 films were grown by ALD (MNT Micro and Nanotech Co., Ltd.) on 3D AAO substrate at 150 °C using tetrakis(dimethylamino)tin ($C_8H_{24}N_4Sn$, TDMAS, 99.999%) and H_2O as the Sn precursor and oxygen source, respectively. The

TDMAS was contained in a bubbler at 70 °C and admitted into the ALD reactor with N_2 carrier gas (20 sccm). High purity N_2 (99.9999%) gas was used as the carrier and purge gas. The SnO_2 ALD pulse sequence consisted of TDMAS injection (700 ms)/purge (30 s)/H_2O (70 ms)/purge (30 s) steps, and the thickness was controlled by the ALD recipe cycles. The SnO_2 films with controlled deposition cycles of 40, 45, and 50 were obtained. Then the as-obtained samples were annealed at 450 °C for 3 h under ambient condition. For Pd decoration, the deposition temperature was set at 200 °C, and palladium(II) hexafluoroacetylacetonate (99.999%) and hydrazine anhydrous were employed as the precursors. The palladium(II) hexafluoroacetylacetonate was contained in a bubbler at 80 °C and admitted into the ALD reactor with N_2 carrier gas (20 sccm). High purity N_2 (99.9999%) gas was used as the carrier and purge gas. The SnO_2 ALD pulse sequence consisted of Palladium(II) hexafluoroacetylacetonate injection (1000 ms)/purge (30 s)/ hydrazine anhydrous (200 ms)/purge (30 s) steps, and the thickness was controlled by the ALD recipe cycles.

Gas Sensor Array Fabrication. To fabricate the gas sensor arrays, the 3D AAO substrates with Pd decorated SnO_2 films were covered by a shadow mask with 2×2 mm^2 square openings (4×4 pixels, Figure S3), and then 150 nm thick Au, Cu, Ni, and Ag were selectively evaporated in the four separated parts as the top electrodes. The backside was covered by a shadow mask with a fishbone shaped opening (bottom electrodes, Figure S3) for 150 nm thick Au evaporation.

Characterization. The morphology of the 3D nanostructured thin films on the AAO substrate was conducted by scanning electron microscope (SEM, JSM-7100F, JEOL) and high-resolution transmission electron microscope (HR-TEM, JEM 2010F, JEOL). X-ray diffraction (XRD) measurements were performed using X'pert Pro (PANalytical) in the 2θ range of 10°–80°.

Gas-Sensing Measurement. The controlled amount of H_2 gas, formaldehyde, toluene, and acetone were introduced using mass flow controllers (MFC1–4), respectively, and every single gas was intermixed with air then injected from MFC5 to control the concentration of the target gas. The gas was introduced into the chamber and the sensor resistance was recorded as a function of time at a fixed voltage of 5 V by a 16-channel analog to digital converter with 16-bit resolution accompanied by a graphic user interface (YAD 16AD, Wuhan Yavii Electronic Technology Co. Ltd.). Air was used for the recovery process and the total flow rate was maintained at 500 sccm. The limit of detection (LOD) in our work is the measured LOD instead of theoretical LOD (three times the relative standard deviation of noise divided by the slope of the linear fit), and the LOD depends on the device itself rather than the measurement set up.

ASSOCIATED CONTENT

ⓈⒾ Supporting Information
The Supporting Information is available free of charge at https://pubs.acs.org/doi/10.1021/acsnano.1c01256.

Figures S1–S17 showing additional experimental results; Tables S1–S7 (PDF)

SINGOR gas leak test (MP4)

SINGOR monitoring system (MP4)

Demonstration of gas leak detection (MP4)

AUTHOR INFORMATION

Corresponding Author
Zhiyong Fan − *Department of Electronic and Computer Engineering and Guangdong-Hong Kong-Macao Joint Laboratory for Intelligent Micro-Nano Optoelectronic Technology, The Hong Kong University of Science and Technology, Kowloon, Hong Kong SAR, China;* ⓘ orcid.org/ 0000-0002-5397-0129; Email: eezfan@ust.hk

Authors
Zhilong Song − *Department of Electronic and Computer Engineering and Guangdong-Hong Kong-Macao Joint Laboratory for Intelligent Micro-Nano Optoelectronic Technology, The Hong Kong University of Science and Technology, Kowloon, Hong Kong SAR, China*

Wenhao Ye − *Department of Electronic and Computer Engineering and Guangdong-Hong Kong-Macao Joint Laboratory for Intelligent Micro-Nano Optoelectronic Technology, The Hong Kong University of Science and Technology, Kowloon, Hong Kong SAR, China*

Zhuo Chen − *Department of Electronic and Computer Engineering and Guangdong-Hong Kong-Macao Joint Laboratory for Intelligent Micro-Nano Optoelectronic Technology, The Hong Kong University of Science and Technology, Kowloon, Hong Kong SAR, China*

Zhesi Chen − *Department of Electronic and Computer Engineering and Guangdong-Hong Kong-Macao Joint Laboratory for Intelligent Micro-Nano Optoelectronic Technology, The Hong Kong University of Science and Technology, Kowloon, Hong Kong SAR, China*

Mutian Li − *Department of Electronic and Computer Engineering and Guangdong-Hong Kong-Macao Joint Laboratory for Intelligent Micro-Nano Optoelectronic Technology, The Hong Kong University of Science and Technology, Kowloon, Hong Kong SAR, China*

Wenying Tang − *Department of Electronic and Computer Engineering and Guangdong-Hong Kong-Macao Joint Laboratory for Intelligent Micro-Nano Optoelectronic Technology, The Hong Kong University of Science and Technology, Kowloon, Hong Kong SAR, China*

Chen Wang − *Department of Electronic and Computer Engineering and Guangdong-Hong Kong-Macao Joint Laboratory for Intelligent Micro-Nano Optoelectronic Technology, The Hong Kong University of Science and Technology, Kowloon, Hong Kong SAR, China;* ⓘ orcid.org/ 0000-0002-5678-5287

Zhu'an Wan − *Department of Electronic and Computer Engineering and Guangdong-Hong Kong-Macao Joint Laboratory for Intelligent Micro-Nano Optoelectronic Technology, The Hong Kong University of Science and Technology, Kowloon, Hong Kong SAR, China*

Swapnadeep Poddar − *Department of Electronic and Computer Engineering and Guangdong-Hong Kong-Macao Joint Laboratory for Intelligent Micro-Nano Optoelectronic Technology, The Hong Kong University of Science and Technology, Kowloon, Hong Kong SAR, China*

Xiaolin Wen − *College of Electronics and Information Engineering, Shenzhen University, Shenzhen 518060, China*

Xiaofang Pan − *College of Electronics and Information Engineering, Shenzhen University, Shenzhen 518060, China*

Yuanjing Lin − *School of Microelectronics and Engineering Research Center of Integrated Circuits for Next-Generation Communications, Ministry of Education, Southern University of Science and Technology, Shenzhen 518055, China*

Qingfeng Zhou − *School of Electric Engineering and Intelligentization, Dongguan University of Technology, Dongguan 523808, China*

Complete contact information is available at:
https://pubs.acs.org/10.1021/acsnano.1c01256

Author Contributions

‡Z.S. and W.Y. contributed equally to the work. Z.F., Z.S., and W.Y. conceived and designed the experiments. Z.S., W.T., and Z.W. performed the device fabrication and measurements. W.Y., Z.C., and M.L. contributed to the system design. Z.C. and C.W. contributed to the machine learning algorithm. S.P. helped with the TEM characterization and result discussions. X.P., X.W., Y.L., and Q.Z. helped with the gas-sensing testing and analysis. Z.S., W.Y., and Z.F. wrote the manuscript. All authors contributed to result discussions and manuscript revisions.

Notes

The authors declare no competing financial interest.

REFERENCES

(1) Wang, B.; Thukral, A.; Xie, Z.; Liu, L.; Zhang, X.; Huang, W.; Yu, X.; Yu, C.; Marks, T.; Facchetti, A. Flexible and Stretchable Metal Oxide Nanofiber Networks for Multimodal and Monolithically Integrated Wearable Electronics. *Nat. Commun.* **2020**, *11*, 2405.

(2) Dincer, C.; Bruch, R.; Costa-Rama, E.; Fernández-Abedul, M.; Merkoçi, A.; Manz, A.; Urban, G.; Güder, F. Disposable Sensors in Diagnostics, Food, and Environmental Monitoring. *Adv. Mater.* **2019**, *31*, 1806739.

(3) Tang, S.; Yang, C.; Su, T.; Yang, T.; Wu, S.; Hsu, Y.; Chen, Y.; Lin, T.; Shen, J.; Lin, H.; Chiu, P.; Kuo, H.; Chueh, Y. Design of Core-Shell Quantum Dots-3D WS$_2$ Nanowall Hybrid Nanostructures with High-Performance Bifunctional Sensing Applications. *ACS Nano* **2020**, *14*, 12668−12678.

(4) Fan, Z.; Lu, J. G. Gate-Refreshable Nanowire Chemical Sensors. *Appl. Phys. Lett.* **2005**, *86*, 123510.

(5) Giraldo, J.; Wu, H.; Newkirk, G.; Kruss, S. Nanobiotechnology Approaches for Engineering Smart Plant Sensors. *Nat. Nanotechnol.* **2019**, *14*, 541.

(6) Chen, Y.; Lee, S.; Su, T.; Wu, S.; Chen, P.; Chueh, Y. Phase-Modulated 3D-Hierarchical 1T/2H WSe$_2$ Nanoscrews by a Plasma-Assisted Selenization Process as High Performance NO Gas Sensors with a Ppb-level Detection Limit. *J. Mater. Chem. A* **2019**, *7*, 22314−22322.

(7) Medina, H.; Li, J.; Su, T.; Lan, Y.; Lee, S.; Chen, C.; Chen, Y.; Manikandan, A.; Tsai, S.; Navabi, A.; Zhu, X.; Shih, Y.; Lin, W.; Yang, J.; Thomas, S.; Wu, B.; Shen, C.; Shieh, J.; Lin, H.; Javey, A.; et al. Wafer-Scale Growth of WSe$_2$ Monolayers toward Phase-Engineered Hybrid WO$_x$/WSe$_2$ Films with Sub-ppb NO$_x$ Gas Sensing by a Low-Temperature Plasma-Assisted Selenization Process. *Chem. Mater.* **2017**, *29* (4), 1587−1598.

(8) Zhu, Y.; Zhao, Y.; Ma, J.; Cheng, X.; Xie, J.; Xu, P.; Liu, H.; Liu, H.; Zhang, H.; Wu, M.; Elzatahry, A.; Alghamdi, A.; Deng, Y.; Zhao, D. Enantioselective Palladium-Catalyzed Intramolecular α-Arylative Desymmetrization of 1,3-Diketones. *J. Am. Chem. Soc.* **2017**, *139*, 10365.

(9) Pan, X.; Liu, X.; Bermak, A.; Fan, Z. Self-Gating Effect Induced Large Performance Improvement of ZnO Nanocomb Gas Sensors. *ACS Nano* **2013**, *7*, 9318−9324.

(10) Yan, J.; Rodrigues, M.; Song, Z.; Li, H.; Xu, H.; Liu, H.; Wu, J.; Xu, Y.; Song, Y.; Liu, Y.; Yu, P.; Yang, W.; Vajtai, R.; Li, H.; Yuan, S.; Ajayan, P. Reversible Formation of g-C$_3$N$_4$ 3D Hydrogels through Ionic Liquid Activation: Gelation Behavior and Room-Temperature Gas-Sensing Properties. *Adv. Funct. Mater.* **2017**, *27*, 1700653.

(11) Fan, Z.; Wang, D.; Chang, P.; Tseng, W.; Lu, J. ZnO Nanowire Field-Effect Transistor and Oxygen Sensing Property. *Appl. Phys. Lett.* **2004**, *85*, 5923.

(12) Li, Z.; Askim, J.; Suslick, K. The Optoelectronic Nose: Colorimetric and Fluorometric Sensor Arrays. *Chem. Rev.* **2019**, *119*, 231.

(13) Jalal, A.; Alam, F.; Roychoudhury, S.; Umasankar, Y.; Pala, N.; Bhansali, S. Prospects and Challenges of Volatile Organic Compound Sensors in Human Healthcare. *ACS Sens.* **2018**, *3*, 1246.

(14) Chen, Z.; Chen, Z.; Song, Z.; Ye, W.; Fan, Z. Smart Gas Sensor Arrays Powered by Artificial Intelligence. *J. Semicond.* **2019**, *40*, 111601.

(15) Hu, W.; Wan, L.; Jian, Y.; Ren, C.; Jin, K.; Su, X.; Bai, X.; Haick, H.; Yao, M.; Wu, W. Electronic Noses: From Advanced Materials to Sensors Aided with Data Processing. *Adv. Mater. Technol.* **2018**, *4*, 1800488.

(16) Chen, J.; Chen, Z.; Boussaid, F.; Zhang, D.; Pan, X.; Zhao, H.; Bermak, A.; Tsui, C.; Wang, X.; Fan, Z. Ultra-Low-Power Smart Electronic Nose System Based on Three-Dimensional Tin Oxide Nanotube Arrays. *ACS Nano* **2018**, *12*, 6079.

(17) Mackin, C.; Schroeder, V.; Zurutuza, A.; Su, C.; Kong, J.; Swager, T.; Palacios, T. Chemiresistive Graphene Sensors for Ammonia Detection. *ACS Appl. Mater. Interfaces* **2018**, *10*, 16169−16176.

(18) Lee, D.; Park, H.; Han, S.; Kim, S.; Huh, W.; Lee, J.; Kim, Y.; Park, M.; Park, W.; Kang, C.; Lee, C. Self-Powered Chemical Sensing Driven by Graphene-Based Photovoltaic Heterojunctions with Chemically Tunable Built-In Potentials. *Small* **2019**, *15*, 1804303.

(19) Lee, J.; Jung, S.; Lee, T.; Jo, J.; Chae, H.; Choi, K.; Kim, J.; Lee, J.; Yang, C.; Baik, J. High-Output Triboelectric Nanogenerator Based on Dual Inductive and Resonance Effects-Controlled Highly Transparent Polyimide for Self-Powered Sensor Network Systems. *Adv. Energy Mater.* **2019**, *9*, 1901987.

(20) Song, Y.; Min, J.; Yu, Y.; Wang, H.; Yang, Y.; Zhang, H.; Gao, W. Wireless Battery-Free Wearable Sweat Sensor Powered by Human Motion. *Sci. Adv.* **2020**, *6*, No. eaay9842.

(21) Song, K.; Zhao, R.; Wang, Z.; Yang, Y. Conjuncted Pyro-Piezoelectric Effect for Self-Powered Simultaneous Temperature and Pressure Sensing. *Adv. Mater.* **2019**, *31*, 1902831.

(22) Leung, S.; Ho, K.; Kung, P.; Hsiao, V.; Alshareef, H.; Wang, Z.; He, J. A Self-Powered and Flexible Organometallic Halide Perovskite Photodetector with Very High Detectivity. *Adv. Mater.* **2018**, *30*, 1704611.

(23) Lin, Y.; Chen, J.; Tavakoli, M.; Gao, Y.; Zhu, Y.; Zhang, D.; Kam, M.; He, Z.; Fan, Z. Printable Fabrication of a Fully Integrated and Self-Powered Sensor System on Plastic Substrates. *Adv. Mater.* **2019**, *31*, 1804285.

(24) Zhu, H.; Lin, H.; Song, Z.; Wang, Z.; Ye, F.; Zhang, H.; Yin, W.; Yan, Y.; Cho, W. Achieving High-Quality Sn-Pb Perovskite Films on Complementary Metal-Oxide-Semiconductor-Compatible Metal/ Silicon Substrates for Efficient Imaging Array. *ACS Nano* **2019**, *13*, 11800.

(25) Oviroh, P.; Akbarzadeh, R.; Pan, D.; Coetzee, R.; Jen, T. New Development of Atomic Layer Deposition: Processes, Methods and Applications. *Sci. Technol. Adv. Mater.* **2019**, *20*, 465.

(26) Meng, X.; Zhang, Y.; Sun, S.; Li, R.; Sun, X. Three Growth Modes and Mechanisms for Highly Structure-Tunable SnO$_2$ Nano-

tube Arrays of Template-Directed Atomic Layer Deposition. *J. Mater. Chem.* **2011**, *21*, 12321.

(27) Kim, S.; Kim, H.; Jung, H.; Park, J.; Seok, T.; Choa, Y.; Park, T.; Lee, S. High-Performance, Transparent Thin Film Hydrogen Gas Sensor Using 2D Electron Gas at Interface of Oxide Thin Film Heterostructure Grown by Atomic Layer Deposition. *Adv. Funct. Mater.* **2019**, *29*, 1807760.

(28) Cho, M.; Zhu, J.; Kim, H.; Kang, K.; Park, I. Half-Pipe Palladium Nanotube-Based Hydrogen Sensor Using a Suspended Nanofiber Scaffold. *ACS Appl. Mater. Interfaces* **2019**, *11*, 13343.

(29) Huang, H.; Gong, H.; Chow, C.; Guo, J.; White, T.; Tse, M.; Tan, O. Low-Temperature Growth of SnO_2 Nanorod Arrays and Tunable *n-p-n* Sensing Response of a ZnO/SnO_2 Heterojunction for Exclusive Hydrogen Sensors. *Adv. Funct. Mater.* **2011**, *21*, 2680.

(30) Li, X.; Liu, Y.; Hemminger, J.; Penne, R. Catalytically Activated Palladium@Platinum Nanowires for Accelerated Hydrogen Gas Detection. *ACS Nano* **2015**, *9*, 3215.

(31) Koo, W.; Kim, Y.; Kim, S.; Suh, B.; Savagatrup, S.; Kim, J.; Lee, S.; Swager, T.; Kim, I. Hydrogen Sensors from Composites of Ultra-small Bimetallic Nanoparticles and Porous Ion-Exchange Polymers. *Chem.* **2020**, *6*, 1−13.

(32) Degler, D.; Wicker, S.; Weimar, U.; Barsan, N. Identifying the Active Oxygen Species in SnO_2 Based Gas Sensing Materials: An Operando IR Spectroscopy Study. *J. Phys. Chem. C* **2015**, *119*, 11792−11799.

(33) Le, H.; Dao, D.; Yu, Y. Superfast and Efficient Hydrogen Gas Sensor Using $PdAu_{alloy}@ZnO$ Core-Shell Nanoparticles. *J. Mater. Chem. A* **2020**, *8*, 12968−12974.

(34) Kim, J.; Mirzaei, A.; Kim, H.; Kim, S. Pd Functionalization on ZnO Nanowires for Enhanced Sensitivity and Selectivity to Hydrogen Gas. *Sens. Actuators, B* **2019**, *297*, 126693.

(35) Johnson, N.; Lam, B.; MacLeod, B.; Sherbo, R.; Moreno-Gonzalez, M.; Fork, D.; Berlinguette, C. Facets and Vertices Regulate Hydrogen Uptake and Release in Palladium Nanocrystals. *Nat. Mater.* **2019**, *18*, 454−458.

(36) Kim, D.; Kim, S.; Shin, H.; Koo, W.; Jang, J.; Kang, J.; Jeong, Y.; Kim, I. High-Resolution, Fast, and Shape-Conformable Hydrogen Sensor Platform: Polymer Nanofiber Yarn Coupled with Nanograined Pd@Pt. *ACS Nano* **2019**, *13*, 6071−6082.

(37) Lee, S. P. Electrodes for Semiconductor Gas Sensors. *Sensors* **2017**, *17*, 683.

(38) Zhu, H.; Li, Q.; Ren, Y.; Gao, Q.; Chen, J.; Wang, N.; Deng, J.; Xing, X. A New Insight into Cross-Sensitivity to Humidity of SnO_2 Sensor. *Small* **2018**, *14*, 1703974.

(39) Song, Z.; Huang, Z.; Liu, J.; Hu, Z.; Zhang, J.; Zhang, G.; Yi, F.; Jiang, S.; Lian, J.; Yan, J.; Zang, J.; Liu, H. Fully Stretchable and Humidity-Resistant Quantum Dot Gas Sensors. *ACS Sens.* **2018**, *3* (5), 1048−1055.

(40) Koo, W.; Choi, S.; Kim, S.; Jang, J.; Tuller, H.; Kim, I. Heterogeneous Sensitization of Metal-Organic Framework Driven Metal@Metal Oxide Complex Catalysts on an Oxide Nanofiber Scaffold toward Superior Gas Sensors. *J. Am. Chem. Soc.* **2016**, *138*, 13431.

(41) Ma, N.; Suematsu, K.; Yuasa, M.; Shimanoe, K. Pd Size Effect on the Gas Sensing Properties of Pd-Loaded SnO_2 in Humid Atmosphere. *ACS Appl. Mater. Interfaces* **2015**, *7*, 15618−15625.

(42) Peng, G.; Tisch, U.; Adams, O.; Hakim, M.; Shehada, N.; Broza, Y.; Billan, S.; Abdah-Bortnyak, R.; Kuten, A.; Haick, H. Diagnosing Lung Cancer in Exhaled Breath Using Gold Nanoparticles. *Nat. Nanotechnol.* **2009**, *4*, 669−673.

(43) Akamatsu, T.; Tsuruta, A.; Shin, W. Selective Detection of Target Volatile Organic Compounds in Contaminated Humid Air Using a Sensor Array with Principal Component Analysis. *Sensors* **2017**, *17*, 1662.